KfK 3233
November 1981

Optical Model Studies of ^{6}Li Elastic Scattering at 156 MeV

J. Cook, H. J. Gils, H. Rebel,
Z. Majka, H. Klewe-Nebenius
Institut für Angewandte Kernphysik
Institut für Radiochemie

Kernforschungszentrum Karlsruhe

KERNFORSCHUNGSZENTRUM KARLSRUHE

Institut für Angewandte Kernphysik
Institut für Radiochemie

KfK 3233

OPTICAL MODEL STUDIES OF ^{6}Li ELASTIC SCATTERING AT 156 MeV

J. Cook*, H.J. Gils, H. Rebel,
Z. Majka**, and H. Klewe-Nebenius

Kernforschungszentrum Karlsruhe GmbH, Karlsruhe

* Wheatstone Laboratory, King's College, Strand, London WC2R 2LS, United Kingdom

Present address: Department of Physics, Florida State University, Tallahassee, Florida 32306, USA

** Jagellonian University, Krakow, Poland

Kernforschungszentrum Karlsruhe GmbH
ISSN 0303-4003

ABSTRACT

Differential cross sections for ^{6}Li elastic scattering at 156 MeV from ^{12}C, ^{40}Ca, ^{90}Zr and ^{208}Pb are presented. The sensitivity to various potential forms is established by using Saxon-Woods, Saxon-Woods-squared, density independent and density dependent folded potentials. The extent to which the experimental data determine the potentials and related quantities is discussed.

UNTERSUCHUNG DES OPTISCHEN MODELLS FÜR DIE ELASTISCHE STREUUNG VON 156 MeV ^{6}Li-IONEN

Differentielle Wirkungsquerschnitte für die elastische Streuung von 156 MeV ^{6}Li Ionen an ^{12}C, ^{40}Ca, ^{90}Zr und ^{208}Pb wurden gemessen und auf der Basis des optischen Modells analysiert. Die Empfindlichkeit auf verschiedene Formen des optischen Potentials wurde untersucht und Saxon-Woods und quadrierte Saxon-Woods Formen, wie auch dichteunabhängige und dichteabhängige Faltungspotentiale betrachtet. Das Ausmaß, zu dem die experimentellen Daten die Potentiale und charakteristische integrale Größen bestimmen, wird diskutiert.

1. INTRODUCTION

The investigation of the elastic scattering of ^{6}Li is of considerable interest from several points of view. ^{6}Li ions occupy an intermediate position between light and heavy ions, and the scattering of these two groups of bombarding projectiles appears to be rather different. In particular, the optical potentials describing the elastic scattering cross sections show qualitative differences. For light ions with high bombarding energies nuclear rainlow scattering is observed, reflecting the refraction due to the real part of the interaction potential and enabling unambiguous determination of the optical potentials [1]. As a consequence, the Saxon-Woods shapes of the potentials - customary at low energies - had to be replaced by more complicated and less constrained potential forms when describing the experimental cross sections. In phenomenological analyses resort has been made to Saxon-Woods forms raised to a power (usually 2) [2] or alternatively to some kind of "model independent" form such as Fourier-Bessel expansions [3] or spline functions [4]. In contrast, even at the highest energies measured, heavy ion scattering potentials seem to be very poorly determined and even the Saxon-Woods form is too powerful. Two parameter ("strength" and "size") exponential potentials are sufficient [5] to reproduce the diffractive, oscillatory angular distributions. With this in mind ^{6}Li scattering exhibits interesting transitional features [6]. Nuclear rainbow scattering has been observed for $^{6}Li + ^{28}Si$ at 135 MeV [6] and 154 MeV [7], and for the case $^{6}Li + ^{12}C$ at 156 MeV [8]. As compared to alpha particle scattering, the refractive behaviour is less distinct, possibly because of the stronger absorption of ^{6}Li, and the sensitivity to the real central potential proves to be reduced. Additionally, for ^{6}Li scattering a possible spin-orbit interaction has to be considered. Up to now, none of the scattering systems studied have been found to be sensitive to including such a term except the ^{12}C target [9].

Reliable optical potentials are of considerable interest not only as a necessary prerequisite for the study of lithium induced nuclear reactions, but also as a basis of a more microscopic understanding of complex particle scattering. With this aim optical model potentials have been generated by folding a realistic G matrix interaction with projectile and target density distributions. These procedures have generally been found to be sucessful in reproducing elastic scattering angular distributions for light and heavy ions [10,11]. The only projectiles whose scattering cross sections could not be reproduced were Li and Be. They appear to be anomalous in the sense that the strength of the effective interaction has to be reduced by a factor of about 2 in order to reproduce the data. The reason for this anomaly is still outstanding and is possibly related to the influence of projectile break up reactions [12].

The highest energy survey of ^{6}Li elastic scattering published so far was at 99 MeV [9]. The cross sections for scattering on ^{12}C showed evidence of the onset of rainbow scattering while scattering from ^{208}Pb was of a Coulomb dominated Fresnel nature.

This paper presents ^{6}Li data at 156 MeV for elastic scattering from ^{12}C, ^{90}Zr and ^{208}Pb targets which are analyzed in conjunction with previously published [11] data for ^{40}Ca. 156 MeV is the highest energy at which ^{6}Li data are currently available and our studies represent the highest energy survey of a number of targets. The work has been conducted to investigate how sensitive the scattering is to different potential forms and how well determined the potentials are. With this in mind a number of phenomenological and folded potential have also been investigated.

2. EXPERIMENTAL PROCEDURE

The experimental basis of the optical model analyses are differential cross sections for elastic scattering measured with the 156 MeV ^{6}Li beam of the Karlsruhe Isochronous Cyclotron. The beam line includes a 150^{o} deflecting magnet - usually operated in dispersive mode for reducing the energy spread of the primary beam. For the ^{6}Li scattering experiments, however, in most cases the analyzing magnet was used in nondispersive mode since the low beam intensity available should not be further reduced. Thus, the energy resolution was not better than 500-600 keV. Inside a 130 cm diameter - scattering chamber four detector telescopes were mounted on one movable arm with fixed angular distance of 1.5° separating adjacent pairs. Each telescope consisted of two silicon surface barrier detectors of thickness 300 μm and 4 mm for measuring the energy loss ΔE and the remaining kinetic energy respectively. The measurement of the integrated beam current was controlled by an additional monitor detector mounted at a fixed scattering angle. The standard electronic setup consisted of a pre-amplifier and a main amplifier for each detector and coincidence equipment for each telescope in order to activate the acquisition system only for true ΔE-E-event pairs. The pulse pairs from the ΔE and E detectors were stored event by event on magnetic tape. The particle identification was performed off-line by software applying the Goulding method. A clear ^{6}Li-^{7}Li separation was achieved over the full energy range. For the scattering experiments natural C and Ca targets, and highly enriched (> 95 %) ^{90}Zr and ^{208}Pb targets with thicknesses of 4-20 mg/cm^2 were used.

Due to the sharp diffraction pattern of the measured cross sections entrance slits were placed in front of the detectors to provide a small angular acceptance of 0.15 - 0.25 degrees.
Thus the total solid angles of the detectors were only 20-30 μsr. This fact together with a very limited beam intensity (1-10 nA) lead to unusually long measuring times and required additional checks for the stability of all components of the experimental arrangement. The difficulties arising from the restricted beam current are reflected by the quality of the data which is obviously poorer than e.g. the 104 MeV alpha particle results (see ref. 13) obtained with the same scattering facilities.

3. OPTICAL MODEL ANALYSIS

3.1 Phenomenological Potentials

It is commonplace in analyses using phenomenological potentials to employ Saxon-Woods forms for the real and imaginary potential. Choosing a volume absorption term as shape of the imaginary part, the total potential is written as

$$U(r) = -V_o \{1+\exp [\frac{r-r_R A^{-1/3}}{a_R}]\}^{-n} - iW_o\{1+\exp [\frac{r-r_I A_T^{-1/3}}{a_I}]\}^{-n} + V_c(r) \tag{1}$$

where A_T is the target mass and n = 1,2 (Saxon-Woods and Saxon-Woods squared form, respectively) have been considered. In general, the shape parameters of the real (r_R, a_R) and imaginary part (r_I, a_I) are varied independently. The Coulomb potential $V_c(r)$ is taken for a point charge interacting with a uniformly charged sphere of the radius $R_c = 1.3\ A_T^{1/3}$ fm. Generating the Coulomb potentials by using realistic charge distributions of the colliding nuclei does not affect the final results significantly, though for heavier target nuclei and for extreme forward angles small effects in the calculated cross sections are evident.

In order to study the occurrence of the discrete ambiguities in the depths of the real potential, for each target a series of searches was made with V_o fixed in 10 MeV intervals from 30-450 MeV. When the radial parameters were fixed at $r_R = 1.3$ fm and $r_I = 1.7$ fm, fitting the remaining potential parameters results always in a minimum with $V_o \approx 100 - 110$ MeV. In the case of ^{12}C where nuclear rainbow scattering is present this is the only χ^2/F minimum and proves to be rather flat (compared to the α-particle scattering case) with correlations between V_o and r_R. The volume integral of the real potential per nucleon pair, $J_R/A_P \cdot A_T$, appears to be well determined. For heavier nuclei discrete ambiguities exist and are characterized by different values of the specific volume integral $J_R/A_P \cdot A_T$. A satisfactory description of the ^{40}Ca data over the entire angular range requires a decreased value of r_R (as compared to $r_R = 1.3$ fm). Tab. 1 compiles the parameter sets resulting from the studies. The sets corresponding to the ^{12}C solution with

$J_R/A_P \cdot A_T \approx 300$ MeV fm^3 show increasing values of V_o for the best fit ^{40}Ca, ^{90}Zr and ^{208}Pb potentials. These fits are displayed (full lines) in fig. 1. As a consequence of the very limited angular range and missing diffraction pattern of the experimental ^{208}Pb cross sections, in this case it is even impossible to discriminate different families of the potential parameters. Any prechosen value of V_o (with adequate adjustments of the remaining parameters) proves to be able to fit the data equally well (though the values of the geometrical parameters may sometimes appear rather strange).

The use of Saxon-Woods squared shapes does not provide significant progress. This is not surprising for the heavier nuclei. Since only the outer most part of the potential distribution is probed this part may be also reproduced with the Saxon-Woods form by changing the Saxon-Woods shape parameters appropriately. The calculations show that the Saxon-Woods solutions with $V_o \approx 110$ MeV, $r_R = 1.3$ fm and $r_I = 1.7$ are practically equivalent to the set $V_o \approx 170$ MeV, $r_R = 1.5$ fm and $r_I = 1.6$ of Saxon-Woods squared forms.

One might expect more sensitivity to different functional forms in the case of scattering from ^{12}C. In contrast to alpha-particle scattering[14], however, the quality of the fit is not improved by introducing the squared Saxon-Woods shape for the ^{6}Li - ^{12}C real optical potential. Although rainbow scattering is evident the central part of the potential seems to remain rather poorly determined so that the central depth V_o remains available for matching the surface as required by the data.

In order to clarify the radial range of sensitivity more clearly and reduce the constraints due to simple prechosen functional forms more generalized forms and model-independent procedures have been successfully introduced, in particular in analyses of elastic alpha particle scattering [3,13]. Such procedures are only reasonable in cases of experimental data with sufficiently high quality and

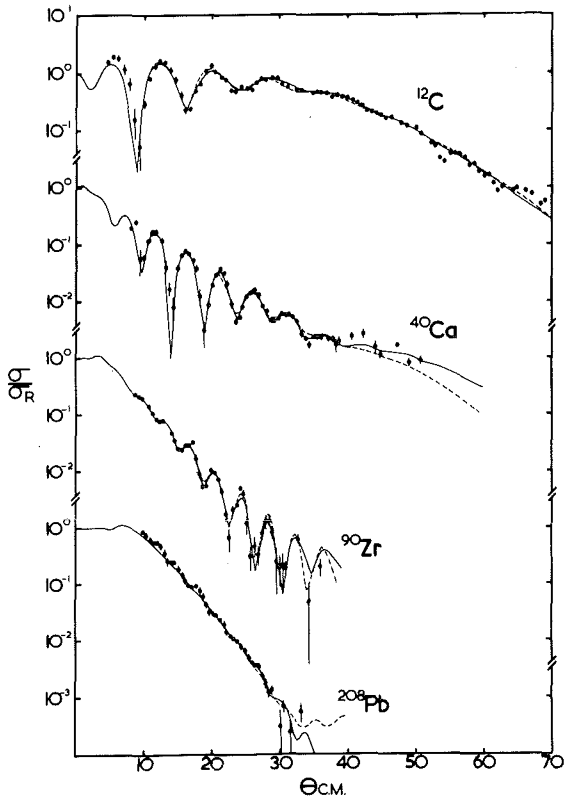

Fig. 1: Optical model fits to ^6Li elastic scattering at 156 MeV using Saxon-Woods (full lines) and Saxon-Woods-squared (dashed lines) real and imaginary potentials. The parameters are given in Table 1.

extending to large angles beyond the nuclear rainbow angle. With our data this is the case for ^6Li scattering from ^{12}C which has been additionally analyzed using the Fourier-Bessel method. This method describes the real potential by adding to a conventional (say Saxon-Woods or squared Saxon-Woods) form an extra-potential given by a Fourier-Bessel series.

Table 1   Phenomenological optical potentials for ^{6}Li elastic scattering at 156 MeV

Target	N	V_o [MeV]	r_R [fm]	a_R [fm]	W_o [MeV]	r_I [fm]	a_I [fm]	J_R/A_PA_T [MeV fm³]	$\langle r_V^2\rangle^{1/2}$ [fm]	J_I/A_PA_T [MeV fm³]	χ^2/F
Saxon-Woods potential											
^{12}C		112.1	$\underline{1.3}$	0.816	32.1	$\underline{1.7}$	0.808	300	3.80	157	6.9
		98.9	1.379	0.781	29.1	1.775	0.782	291	3.80	155	6.9
^{40}Ca		112.0	$\underline{1.3}$	0.899	30.0	$\underline{1.7}$	0.863	241	4.80	125	7.9
		145.0	1.127	1.037	21.65	1.837	0.718	248	4.87	105	5.5
		182.1	1.135	0.934	31.3	1.687	0.844	292	4.59	127	4.0
^{90}Zr		109.4	$\underline{1.3}$	0.853	22.2	$\underline{1.7}$	0.910	203	5.51	87	2.9
		201.0	1.187	0.842	20.37	1.709	0.921	293	5.17		2.3
^{208}Pb		113.5	$\underline{1.3}$	0.673	16.2	$\underline{1.7}$	0.995	187	6.47	61	1.2
		240	1.170	0.766	20.0	1.554	1.015	301	6.08	59	2.0
Saxon-Woods-squared potentials											
^{12}C		170.0	$\underline{1.5}$	1.331	87.0	$\underline{1.6}$	0.788	320	3.72	178	9.1
		125.4	1.593	1.255	50.0	1.783	1.474	270	3.70	253	6.9
		*126.5	1.614	1.237	38.9	1.570	0.852	280	3.70	164	6.9
^{40}Ca		170.0	$\underline{1.5}$	1.225	76.2	$\underline{1.6}$	1.022	286	4.47	116	13.7
		312.8	1.123	1.76	34.9	1.88	1.35	271	4.22	117	5.4
^{90}Zr		170.0	$\underline{1.5}$	0.958	54.1	$\underline{1.6}$	1.229	298	5.23	112	3.6
^{208}Pb		170.0	$\underline{1.5}$	0.272	44.5	$\underline{1.6}$	1.159	367	6.72	97	1.5

*Saxon-Woods form for the imaginary part - Underlined numbers indicate quantities kept fixed in the particular search.

$$U(r) = U_o(r) + \sum_{n=1}^{N} b_n \, j_o \, (q_n \, r) \tag{2}$$

The quantities j_o are spherical Bessel functions, $q_n = n\pi/R_{cut}$ and R_{cut} is a suitably chosen cut-off radius beyond which the extra potential vanishes. The N coefficients b_n are determined by least-squares fit to the data (usually N = 10 - 13). Within the framework of the FB-procedure the mean square uncertainty of the potential value at the distance r is given by

$$[\delta U(r)]^2 = 2 \sum_{m,n=1} \langle \delta b_m \, \delta b_n \rangle_{av} \, j_o \, (q_m r) \; j_o(q_n r) \tag{3}$$

with $\langle \delta b_m \, \delta b_n \rangle_{av}$ being the correlation matrix between the coefficients b_n. The FB method has been shown to lead to very good values of χ^2/F and to well defined integral quantities of the potential, and at the same time providing realistic estimates of errors [3).]

Fig. 2 displays the fit obtained for the ^{12}C data when applying the Fourier-Bessel method. The improvement in the values of χ^2/F is obvious. It should be noted that the shape of the imaginary potential was of the Saxon-Woods form, while the best-fit Saxon-Woods squared form was taken for U_o in eq. (2).

The resulting real potential distribution is shown in fig. 3. The hatched area represents the error band indicating the reduced sensitivity of the experimental cross section to the inner part of the potential. For comparison the best-fit (real) Saxon-Woods potential is displayed which approximates rather well the FB potential.

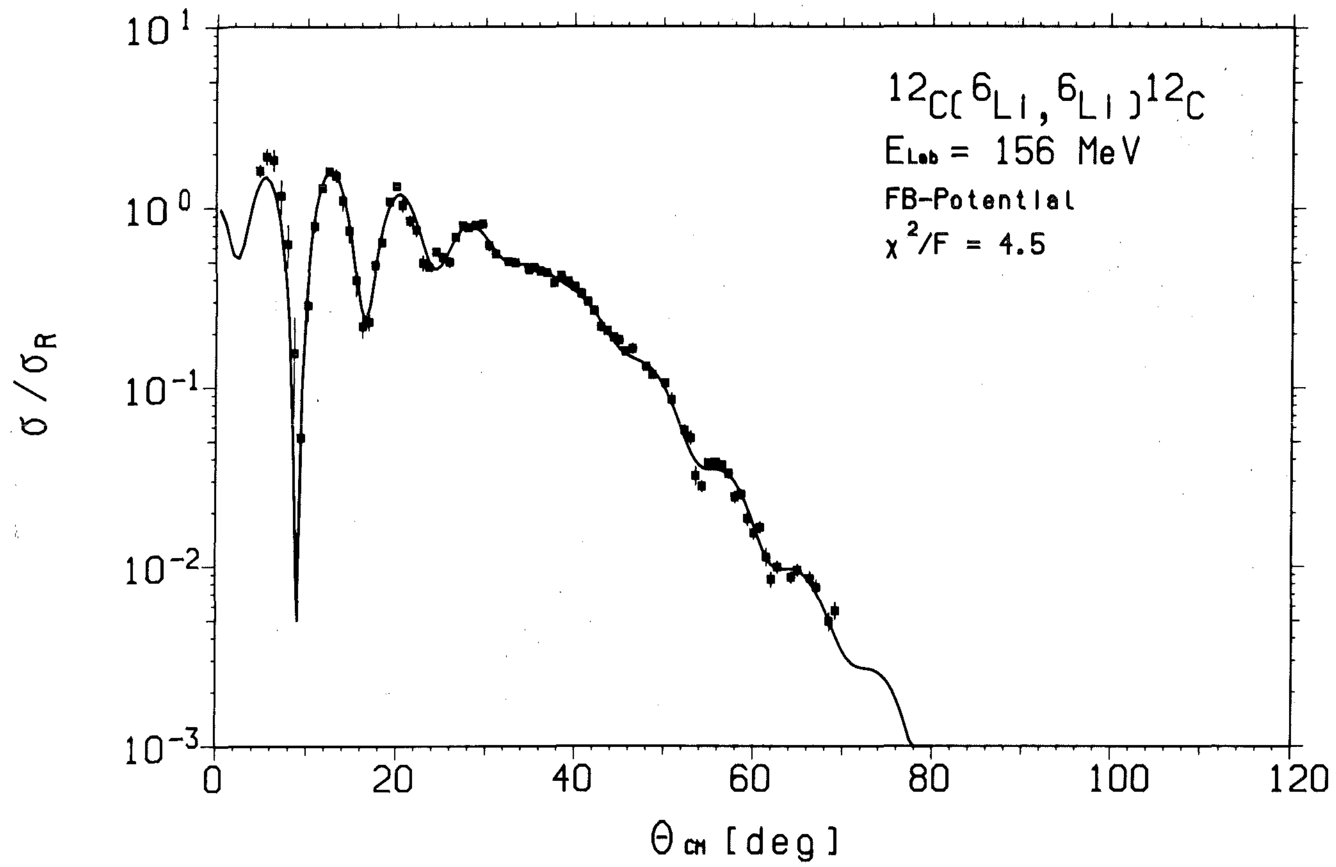

Fig. 2: $^{12}C(^6Li,^6Li)^{12}C$ at 156 MeV:
Experimental cross sections and theoretical description by a Fourier-Bessel potential (real part of the optical potential).

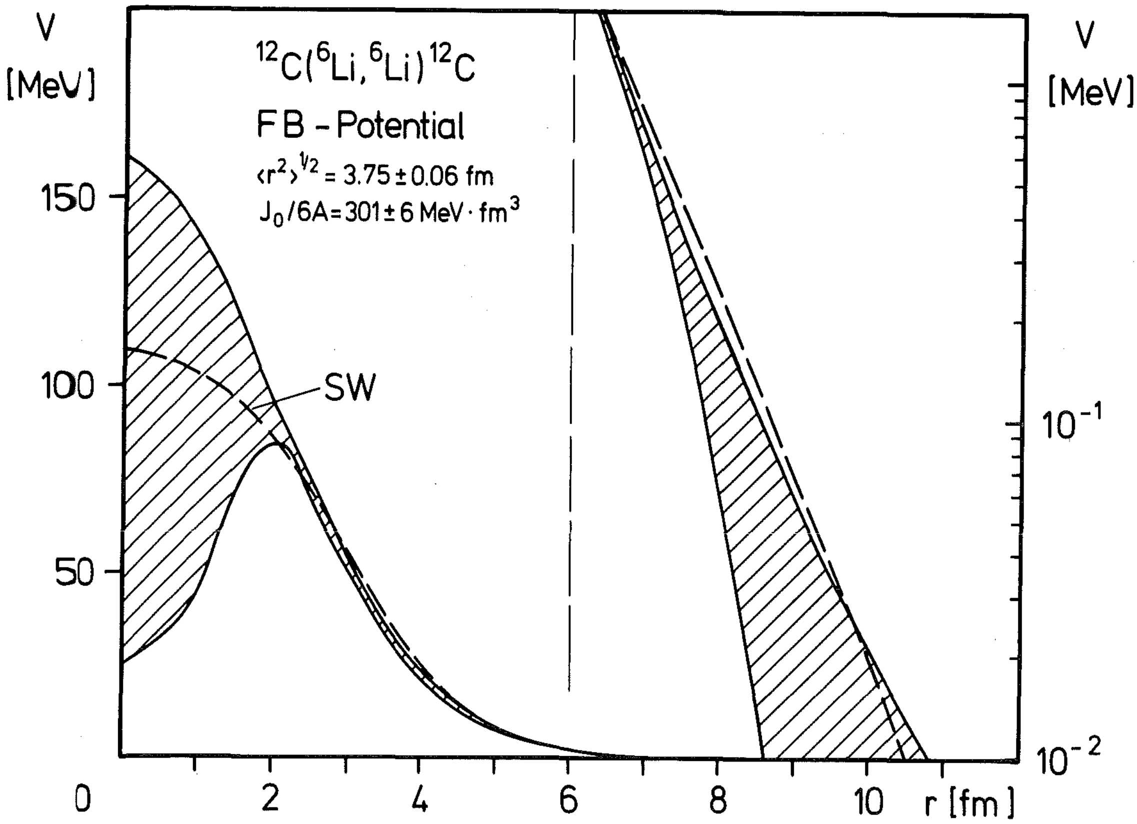

Fig. 3: Real optical potential for elastic scattering of 156 MeV ^{6}Li scattering from ^{12}C determined by the Fourier-Bessel method.

3.2 Folded Potentials

In order to achieve a more microscopic description of nuclear reaction processes it is desirable to relate the nucleus-nucleus optical potential to the fundamental nucleon-nucleon interaction. A step towards this have been the double folding models [9-11,15] in which an effective nucleon-nucleon interaction $V_{eff}(\vec{r})$ is integrated over the densities of both the projectile $\rho_P(r)$ and target $\rho_T(r)$ nuclei

$$V_F(r) = \int dr_P \int dr_T \; \rho_P(\vec{r}_P) \; \rho_T(\vec{r}_T) \; V_{eff}(\vec{r}+\vec{r}_P-\vec{r}_T) \qquad (4)$$

The Bertsch M3Y interaction [16] has been widely applied for both light and heavy ions. Its explicit form is

$$V_{eff}(r) = V_{M3Y}(r) = 7999 \, \frac{e^{-4r}}{4r} - 2134 \, \frac{e^{-2.5r}}{2.5r} - 262 \, \delta(r) \qquad (5)$$

where the two Yukawa functions account for the direct part and the zero-range term represents single nucleon exchange.

In fitting data the real folded potential is multiplied by a normalization factor N and a Saxon-Woods imaginary term is added. Thus the total potential used is

$$U(r) = N \, V_F(r) - i \, W_o \, \left\{1+\exp\left[\frac{r-r_I A_T^{1/3}}{a_I}\right]\right\}^{-1} + V_c(r) \qquad (6)$$

For nucleons, alpha-particles and heavy ions ($A_P \geq 10$) at energies up to 20 MeV/nucleon the folded potential is successful in the sense that it predicts angular distributions that fit the data with N ≈ 1.0. However, for ^{6,7}Li [10,11,17] and ^{9}Be [10,18] projectiles (and even for tritons and ^{3}He [19]) the optical potential based on a folding model has been found unsuccessful since values of N much less than unity are required in order to fit the data [10,9]. These findings are confirmed by the present 156 MeV ^{6}Li data.

In addition to using a realistic nucleon-nucleon interaction to generate folded potentials, realistic density distributions are required. Satchler and Love [10] have found that the most important quantitiy is the rms radius. All the density distributions used in this work accurately reproduce charge distributions or form factors from high enery electron scattering and have rms charge radii which agree well with measured values. For the projectile density the ^{6}Li charge distribution determined by Suelzle et al. [20] has been used, and the proton charge distribution has been unfolded as described in ref. 10. The neutron and proton matter distributions were then assumed to be identical.

An independent particle model calculation was made for the density of ^{12}C following Satchler's [21] "standard" matter distribution. The semi-self-consistent calculations of Brown et al. [22] were used for the density distribution of ^{40}Ca and unpublished Hartree-Fock calculations [23] for ^{90}Zr and ^{208}Pb. The final parameters of the cross section calculations are given in tab. 2 and measured and calculated cross sections are compared in fig. 4. The agreement (after the effective interaction had been reduced by N fitting to about 0.6) with the experimental results is a little worse than with the phenomenological Saxon-Woods potential. There might be a tendency for both N and W_o to decrease for the heavier targets. However, for ^{90}Zr and particularly for ^{208}Pb values of N over a range of at least 0.5 - 0.6 give satisfactory fits, and therefore

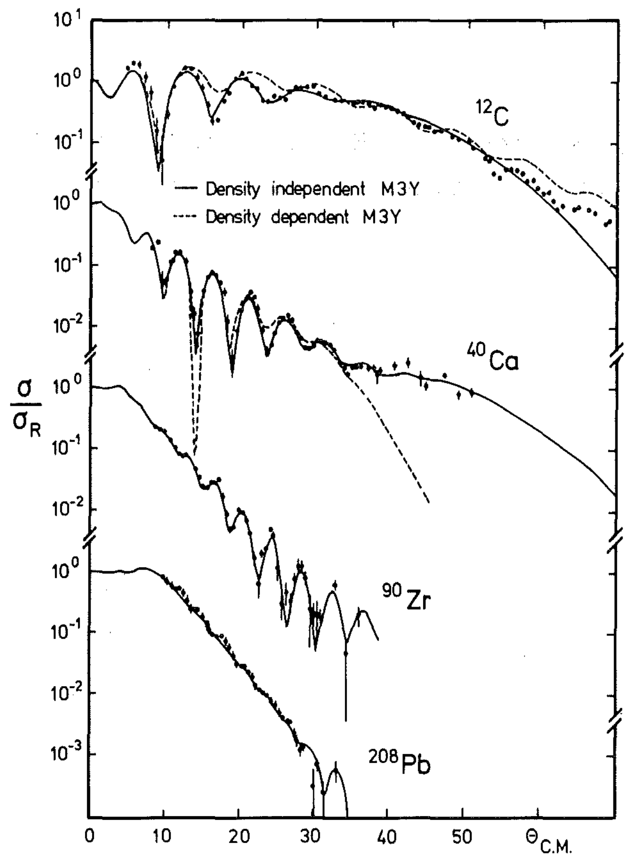

Fig. 4: Optical model fits to ^{6}Li elastic scattering at 156 MeV using folded real potentials and Saxon-Woods imaginary potentials. The full and dashed lines (for ^{12}C and ^{40}Ca only) show the results of calculations using density independent and density dependent versions of the M3Y interaction, respectively. The parameters are given in Tab. 2.

Table 2   Optical potentials in the folding model approach for ^{6}Li elastic scattering

Target	N	W_o [MeV]	r_I [fm]	a_I [fm]	J_R/A_PA_T [MeV fm³]	$\langle r_V^2\rangle^{1/2}$ [fm]	J_I/A_PA_T [MeV fm³]	χ^2/F
Density independent M3Y potentials								
^{12}C	0.793	33.34	1.693	0.830	323	3.72	164	12.0
^{40}Ca	0.690	31.86	1.648	0.950	281	4.45	127	6.9
^{90}Zr	0.612	29.05	1.592	0.977	250	5.16	97.0	2.5
^{208}Pb	0.562	14.51	$\underline{1.7}$	0.835	229	6.28	53.1	1.5
Density dependent M3Y potentials								
^{12}C	0.800	65.19	$\underline{1.7}$	0.538	266	2.45	266	67.0
^{40}Ca	0.749	25.35	$\underline{1.7}$	0.939	223		109	19.0

Underlined numbers indicate quantities kept fixed in the particular search.

Table 3   Phenomenological optical potentials for 156 MeV ^{6}Li scattering with a complex spin orbit term included

Target	V_o [MeV]	r_R [fm]	a_R [fm]	W_o [MeV]	r_I [fm]	a_w [fm]	V_{SO} [MeV]	r_{SO} [fm]	a_{SO} [fm]	W_{SO} [MeV]	r'_{SO} [fm]	a'_{SO} [fm]	J_R/A_PA_T [MeV]	χ^2/F
^{12}C	104.2	1.385	0.803	21.7	1.940	0.764	2.456	1.378	0.309	0.569	1.867	0.353	315	3.6
^{40}Ca	182.1	1.157	0.914	31.6	1.722	0.830	1.414	1.631	0.396	0.317	2.055	0.402	301	3.3

no definite conclusion can be made about the variation of N with the target mass. It would appear that there is a tendency for the real and imaginary strengths to be correlated when the shape of the real potential is fixed through the choice of a folded form.

Folded potentials generated using the M3Y *density independent* interaction are deep in the centre ($V_F(r=0) \approx 65\ A_P$ MeV). Particularly at high energies when there is considerable overlap between the two nuclei it may be considered more appropriate to use a density dependent interaction. In the local density approximation, density dependence is often conveniently included by the parametrization

$$V_{eff}(r) = v_1(r) + v_2(r)\ e^{-\beta\rho(r)} \tag{7}$$

where $v_1(r)$ and $v_2(r)$ are density independent terms.
There is some question as what to use for the actual value of the density $\rho(r)$. Most studies have simply taken the sum of the projectile and target densities: $\rho(r) = \rho_P(r) + \rho_T(r)$. Majka et al. [11] found that for 104 MeV alpha particles the normalization of the potential then became greater than unity. They introduced a factor $m(0 \leq m \leq 1)$ to account for the compression of the projectile in the collision ("intermediate approximation") and wrote

$$\rho(r) = m\ \rho_P(r) + \rho_T(r).$$

Potential normalizations of unity were obtained in the intermediate approximation of m = 0.5. However, for ^{6}Li scattering even in the "sudden" approximation (m = 1) the normalization factor N remained < 1.0.
Satcher and Love [10] introduced a density dependent interaction (called DDD interaction in ref. 10) by

$$\begin{aligned} v_1(r) &= 6839\ \frac{e^{-4r}}{4r} - 1887\ \frac{e^{-2.5r}}{2.5r} - 213\ \delta(r) \\ v_2(r) &= 6893\ \frac{e^{-4r}}{4r} - 1.938\ \frac{e^{-2.5r}}{2.5r} \end{aligned} \tag{8}$$

with $\beta = 41.4\ \text{fm}^3$. At zero density the DDD interaction is much stronger than the M3Y, but it rapidly decreases in strength as the density increases and becomes comparable to M3Y for densities around one third of normal density. The resulting folded potentials for heavy ion systems are a few percent weaker at small r but are very similar to the M3Y potentials near the strong absorption radius. Because of the similarity of DDD and M3Y potentials, the DDD interaction has not been applied in our studies.

An alternative density dependent parametrization [24] is one in which the M3Y interaction is used for both $v_1(r)$ and $v_2(r)$ in eq. (7). The interaction is now written as

$$V_{eff}(r) = V_{M3Y}(r)\ \{c\ [1 + 6.20\ e^{-8.64}\ (\rho_P(r) + \rho_T(r))]\} \qquad (9)$$

and is referred to here as the *density dependent* M3Y interaction to distinguish it from the normal density independent M3Y interaction of eq. (3). Kobos [25] has found for alpha particles and Satchler [26] for heavy ions that $N \approx 1$ results if c is chosen so that the factor in curly brackets is unity when $\rho_P + \rho_T = 1/2\ \rho_o$, where ρ_o ($= 0.17\ \text{fm}^{-3}$) is normal nuclear density. Thus c = - 0,251 is required. It would therefore appear that the M3Y interaction is suitable for 1/2 nuclear densities, not 1/3 as the similarity with the DDD interaction implies. At zero densities the density dependent M3Y interaction is almost twice as strong as the density independent version, but has only 60 % of the strength for full nuclear densities.

We investigated the effective interaction defined by eq. 9 only in the case of scattering from ^{12}C and ^{40}Ca because of the reduced sensitivity of the experimental cross sections for the heavier targets. Again $N < 1.0$ is required, but much poorer fits were obtained than with any of the previous potential forms. Therefore it may be concluded that the density dependence of the form parametrized by eq. (9) is unsucessful for ^{6}Li. Nevertheless, the problem with density dependence of ^{6}Li scattering potentials appears to be related to nuclear rainbow scattering as it does for alpha particle scattering [27]. For ^{6}Li scattering from ^{12}C the well defined rainbow scattering tries to force the parameters in such a way that the rainbow itself is well fitted, and this causes even the forward angle part of the angular distributions to be incorrectly predicted. It should be noted that the small amplitude oscillations for $\Theta > 50^0$ are suggested by the density dependent calculations (may be indirectly, as consequence of the somewhat strange strength of the imaginary potential), a feature which none of the previously potentials (neglecting spin-orbit interaction) predicted, except the flexible FB-potential.

3.3 Effects of a Spin-Orbit Potential

Since ^{6}Li has a spin of unity it has a spin-orbit component in its optical potential which may have an effect on the calculated angular distributions and the resulting potential parameters. The effect of including a spin-orbit term was studied by adding to the central potential a Thomas form

$$U_{LS} = \lambda_\pi^2 \left(V_{SO} \cdot \frac{1}{r}\frac{df(r)}{dr} + i\, W_{SO}\frac{1}{r}\frac{dg(r)}{dr}\right) (\vec{L}\cdot\vec{S}) \qquad (10)$$

with f(r) and g(r) specified by Saxon-Woods shapes. It was found that in the case of scattering from ^{12}C the angular distributions are clearly influenced (see also ref. 9), and that the effects for ^{40}Ca are considerably smaller (if at all significant, see also ref. 11). Since there is a feedback of the spin-orbit term to the best-fit parameters of the central potential (in particular to the imaginary part) any constraint in the potential parameters appears to be very delicate and may lead to wrong impressions about the necessity to introduce a L·S-term. As only scattering cross sections of unpolarized projectiles are considered, the only criterium indicating the presence of a nonnegligible spin-orbit interaction comes from the improvement of the fit when allowing some readjustment of the central potential parameters. This is just the case of ^{6}Li scattering from ^{12}C. With the (Saxon-Woods potential) parameters given in tab. 3 the phenomenological best-fit L·S potential decreases χ^2/F by about a factor of two (only 25 % in the case of ^{40}Ca, see ref. 11) reproducing the cross sections with the same quality as the Fourier Bessel potential, even the wiggles at large scattering angles (fig. 5). As compared to the pure central Saxon-Woods potential (tab. 1) the real part remains nearly unaffected by including the L·S term. However, the sucess

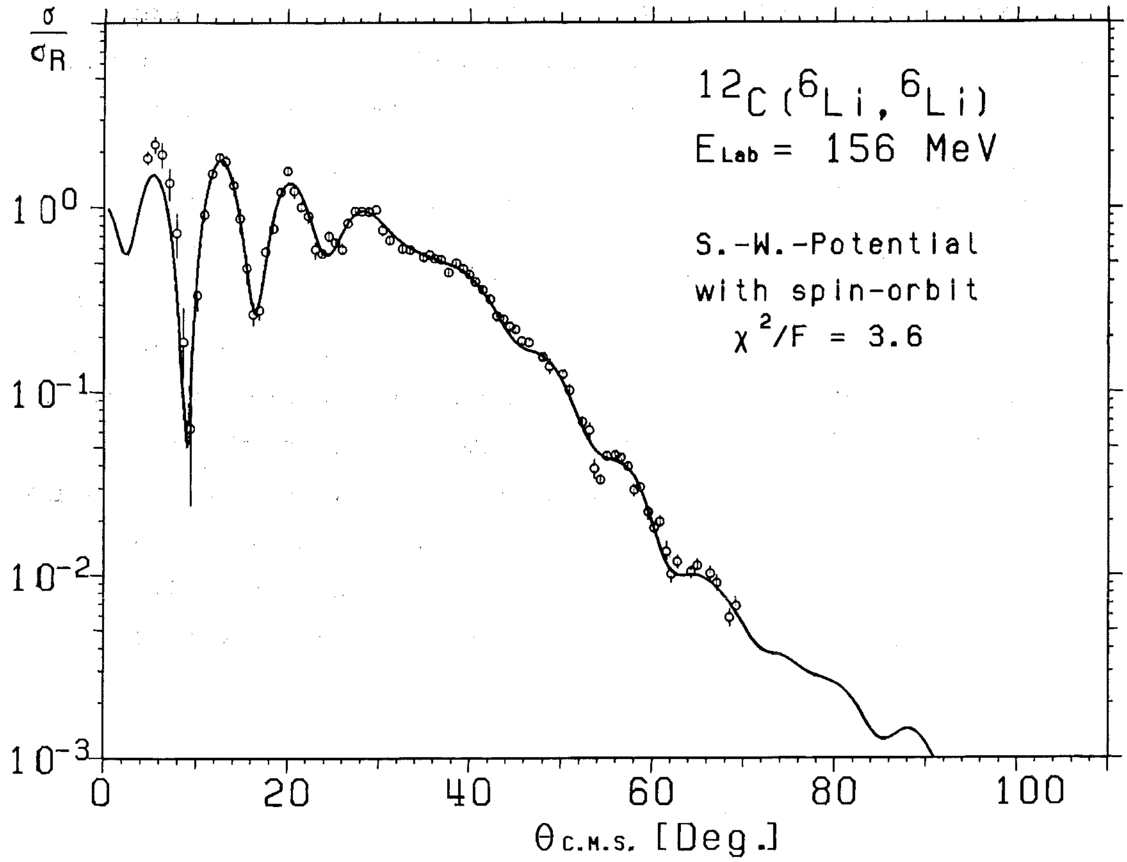

Fig. 5: Differential cross sections for elastic ^{6}Li scattering from ^{12}C with a complex spin-orbit potential included in the calculations.

of the Fourier Bessel potential without any L·S term shows that a central potential with sufficient flexibility is able to absorb not too large spin orbit effects. Therefore we conclude that the problem remains unresolved and it is unlikely to be solved on this basis.

4. DISCUSSION

Considering the question of sensitivity of 156 MeV ^{6}Li scattering to the shape of the optical potential the most direct information is provided in the case of scattering from ^{12}C for which a Fourier-Bessel potential analysis was feasible (fig. 3). The radial range between 2.5 and 7.5 fm, where the real potential appears to be will determined is reproduced with nearly equal quality by Saxon-Woods, Saxon-Woods squared and density independent folded forms (fig. 6), with almost equally good fits to the experimental cross sections. Only the density dependent folded potential using a modified M3Y interaction differs and is not able to produce agreement with the measurements, so that this particular parametrisation can be definitively excluded. Generalizing the observation with the ^{12}C target that the real potential is well determined in just that region where different potential forms, if leading to similar fits, coincide, we may conclude from fig. 6 that the range of sensitivity is somewhat more shifted to larger radii in ^{40}Ca. Of course, for the heavier nuclei it would be desirable to extend the measurements of the differential cross sections to larger angles at a higher level of precision in order to increase the sensitivity. However, noting the results in fig. 6

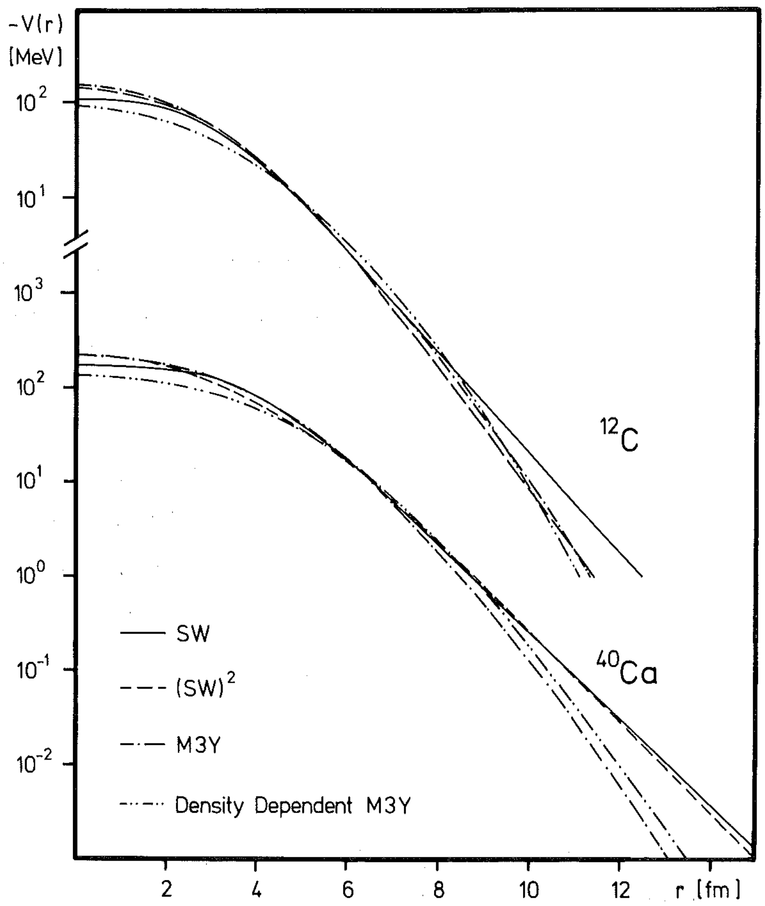

Fig. 6: Comparison of various types of real potential for ^{12}C and ^{40}Ca targets.

we emphasize also the importance of the tail region at larger r values requiring precise measurements of the extreme forward angle distributions and careful analyses of the competition of Coulomb and nuclear scattering. Such additional studies might eventually be able to discriminate different slopes of the outer most tails.

Discussing the folding model approach more specifically we should expect that the results for any density independent calculation (actually a little worse compared to the phenomenological results) could be improved by including saturation effects. With the density dependent M3Y interaction the contrary had been the case. For the ^{40}Ca data a different approach has been reported [11] to be more successful. Applying the same approach, however, the ^{12}C cross sections could not be satisfactorily described. As a plausible explanation for this fact the cluster structure of both the projectile and the target nuclei has been discussed [28]. Indeed, a double folding cluster model [28] using phenomenological alpha particle alpha particle and deuteron-alpha particle interactions improved the results considerably, with values of $\langle r_v^2 \rangle^{1/2}$ and of the specific volume integral very close to those of the phenomenological Saxon-Woods potential. The small amplitude oscillations of the experimental cross sections at $\Theta > 50^o$ are not reproduced. If confidence is placed in such a double folding cluster model, our studies of spin orbit effects would suggest that the wiggles are an indication of a spin orbit interaction. But as discussed above any further conclusion of this kind depends on what we accept for the central potential.

Useful quantities for characterizing the optical potential are the volume integrals per interacting nucleon, the values of which are presented in the tables. These specific volume integrals for the real part of the ^{12}C and ^{40}Ca potentials are well determined within a particular family, and the mass independent value of about 300 MeV fm^3 possibly indicates the relevant family. The real volume integrals for heavier targets are consistent with either this value or (tentatively) with values decreasing with increasing mass approximately as $J_R/A_P \cdot A_T \approx 380 - 27\ A_T^{1/3}$ MeV fm^3. More sensitive data are needed to establish definitely the variation of the real volume integral with target mass. However, for all targets the value obtained for ^6Li scattering is lower than for protons [29] and other lighter particles at the same incident velocity.

The volume integral of the imaginary potential appears to be rather well determined even for the heavier targets and can be well described by the relationship $J_I/(A_P \cdot A_T) \approx 235 - 31\ A_T^{1/3}$ MeV fm^3. For a particular target the rms radii of the real potentials are very similar for the SW, SW^2 and M3Y forms, indicating that they are well determined. However, much smaller values result for the density dependent M3Y potentials, which may be a reason for their failure to fit the data.

5. CONCLUSIONS

The elastic scattering cross sections for ^6Li + ^{12}C, ^{40}Ca, ^{90}Zr and ^{208}Pb have been measured at 156 MeV and analyzed using different forms of the optical potential. The occurrence of rainbow scattering for ^{12}C does not enable the real potential to be determined at small radii as well as observed in the comparable case of 104 MeV alpha particle scattering [14]. Saxon-Woods, Saxon-Woods-squared and folded potentials generated by the M3Y interaction prove to be nearly equivalent in the potential region probed by the scattering data. The folded potentials must be multiplied by N $\approx$ 0.6 - 0.7: another confirmation of the "anomaly" for ^6Li scattering. The measured differential cross sections for the scattering from ^{12}C are sensitive to the inclusion of a spin orbit potential, and if a Saxon-Woods shape is accepted for the central potential, a spin orbit term of reasonable strength improves the agreement between theoretical and experimental results significantly. The analysis using the Fourier-Bessel method, however, shows that a similar improvement can be provided by a less simple shape of the real central potential. Somewhat unexpectedly the volume integral of the imaginary potential appears to be well determined, and decreases with mass number. This is just an observation and has not been studied systematically.

ACKNOWLEDGEMENTS

The continuous interest of Prof. Dr. G. Schatz in our studies is gratefully acknowledged. We thank the cyclotron staff for their efforts in providing the ^{6}Li beam. Dr. J. Buschmann and S. Zagromski have participated in measuring the elastic scattering cross sections. One of us (J.C.) acknowledges financial support from the Science Research Council in the form of a postgraduate studentship, and the hospitality received at Karlsruhe while working on this paper. The authors are also grateful to Dr. B.A. Brown for use of his results of nuclear density distributions.

REFERENCES

1) D.A. Goldberg, S.M. Smith and G.F. Budzik,
Phys. Rev. C10 (1974) 1362
2) D.A. Goldberg, Phys. Lett. 55B (1975) 59
A. Budzanowski, K. Grotowski, M. Grzywacz and A. Strzalkowski,
Progr. Rep. Inst. Nucl. Phys. Cracow (1972) (unpublished)
3) E. Friedman and C.J. Batty, Phys. Rev. C17 (1978) 34
4) L.W. Put and A.M. Paans, Nucl. Phys. A291 (1977) 93
5) M. Lozano and G. Madurga, Nucl. Phys. A334 (1980) 349
6) R.M. de Vries, D.A. Goldberg, J.W. Watson, M.S. Zisman and
J.G. Cramer, Phys. Rev. Lett. 39 (1977) 450
7) P. Schwandt, S. Kailas, W.W. Jacobs, M.D. Kaitchuk, W. Ploughe,
and P.P. Singh, Phys. Rev. C21 (1980) 1656
8) H.J. Gils, J. Buschmann, Z. Majka, B. Neumann, H. Rebel,
S. Zagromski, and H. Klewe-Nebenius, in "Heavy Ion Physics"
eds. A. Berinde, V. Ceausescu, and I.A. Dorobantu,
(Proc. Predeal Int. School, Romania, 1978) p. 1133
9) D.P. Stanley, F. Petrovich and P. Schwandt,
Phys. Rev. C22 (1980) 1357
10) G.R. Satchler and W.G. Love, Phys. Reports 55 (1979) 183;
Phys. Lett. 65B (1976) 415
11) Z. Majka, H.J, Gils and H. Rebel, Z. Phys. A288 (1978) 139
12) I.J. Thompson and M.A. Nagarajan, Phys. Lett. (in press)
13) H.J. Gils, E. Friedman, H. Rebel, J. Buschmann, S. Zagromski,
H. Klewe-Nebenius, B. Neumann, R. Pesl, and G. Bechtold,
Phys. Rev. C21 (1980) 1239
14) H.J. Gils and H. Rebel, Annual Report 1978-79, Kernforschungszentrum Karlsruhe, KfK-Report 2868 (1979)
15) A. Budzanowski, A. Dudek, K. Grotowski, A. Strzalkowski,
Phys. Lett. 32B (1970) 431
16) G. Bertsch, J. Borysowicz, H. McManus, and W.G. Love,
Nucl. Phys. A284 (1977) 399
17) C.W. Glover, R.I. Cutler and K.W. Kemper,
Nucl. Phys. A341 (1980) 137,
M.F. Steeden, S.J. Cartwright, J. Coopersmith, N.M. Clarke
and R.J. Griffiths, J. of Phys. G6 (1980) 501,
J. Cook, N.M. Clarke and R.J. Griffiths, Nucl. Phys. A357
(1981) 246

18) G.R. Satchler, Phys. Lett. 83B (1979) 284
J.S. Eck, T.R. Ophel, P.D. Clark and D.C. Weisser, Nucl. Phys. A334 (1980) 519

19) J. Cook and R.J. Griffiths, Nucl. Phys. A 366 (1981) 27

20) L.R. Suelzle, M.R. Yearian and H. Crannell, Phys. Rev. 162 (1967) 992

21) G.R. Satchler, Nucl. Phys. A329 (1979) 233

22) B.A. Brown, S.E. Massen and P.E. Hodgson, J. Phys. G5 (1979) 1655

23) B.A. Brown, private communication (1980)

24) W.G. Love, Phys. Lett. 72B (1977) 4

25) A.M. Kobos, private communication (1981)

26) G.R. Satchler, private communication (1980)

27) E. Friedman, H.J. Gils, H. Rebel and Z. Majka, Phys. Rev. Lett. 41 (1978) 1220

28) Z. Majka, H.J. Gils and H. Rebel, preprint 1981 (submitted for publication)

29) J.P. Jeukenne, A. Lejeune and C. Mahaux, Phys. Rev. C16 (1977) 80

Appendix: Tables of differential cross sections

SCATTERING OF 6-LI PARTICLES ON 12-C

ELAB = 156.000 MEV Q = 0.0 MEV I = 0 +

ECM = 103.912 MEV K = 4.4635/FERMI ETA = 0.55663

LABORATORY DATA THETA DEGREE	SIGMA MB/SR	DSIGMA %	RUTHERFORD SIGMA/SR	CM DATA THETA DEGREE	SIGMA MB/SR	DSIGMA MB/SR
3.14	4.869E+04	6.7	1.608E+00	4.74	2.136E+04	1.441E+03
3.64	3.227E+04	9.4	1.925E+00	5.50	1.417E+04	1.325E+03
4.14	1.850E+04	13.0	1.846E+00	6.25	8.123E+03	1.055E+03
4.70	7.080E+03	20.8	1.171E+00	7.09	3.111E+03	6.476E+02
5.20	2.529E+03	26.1	6.298E-01	7.86	1.112E+03	2.907E+02
5.70	4.354E+02	56.2	1.558E-01	8.60	1.916E+02	1.076E+02
6.20	1.045E+02	63.4	5.258E-02	9.37	4.600E+01	2.917E+01
6.68	4.246E+02	18.2	2.871E-01	10.08	1.871E+02	3.404E+01
7.19	8.726E+02	6.9	7.934E-01	10.86	3.848E+02	2.649E+01
7.75	1.054E+03	2.0	1.289E+00	11.70	4.652E+02	9.284E+00
8.25	1.013E+03	2.9	1.590E+00	12.45	4.474E+02	1.298E+01
8.75	7.618E+02	7.5	1.513E+00	13.20	3.369E+02	2.524E+01
9.25	4.429E+02	11.7	1.098E+00	13.95	1.961E+02	2.302E+01
9.74	2.447E+02	13.8	7.475E-01	14.70	1.085E+02	1.499E+01
10.25	1.061E+02	18.4	3.963E-01	15.46	4.708E+01	8.676E+00
10.75	4.857E+01	13.4	2.194E-01	16.21	2.158E+01	2.892E+00
11.21	4.360E+01	9.9	2.325E-01	16.90	1.940E+01	1.929E+00
11.70	7.590E+01	5.7	4.806E-01	17.64	3.381E+01	1.942E+00
12.19	8.621E+01	5.0	6.429E-01	18.38	3.845E+01	1.906E+00
12.75	1.218E+02	3.2	1.087E+00	19.22	5.444E+01	1.722E+00
13.25	1.273E+02	3.9	1.323E+00	19.97	5.695E+01	2.238E+00
13.70	8.729E+01	7.8	1.038E+00	20.65	3.912E+01	3.056E+00
14.25	6.107E+01	6.3	8.483E-01	21.47	2.742E+01	1.715E+00
14.75	4.736E+01	7.2	7.546E-01	22.21	2.130E+01	1.542E+00
15.25	2.720E+01	9.2	4.949E-01	22.96	1.226E+01	1.129E+00
15.71	2.289E+01	3.1	4.688E-01	23.65	1.033E+01	3.195E-01
16.25	2.434E+01	2.7	5.699E-01	24.46	1.101E+01	2.953E-01
16.75	2.017E+01	3.9	5.328E-01	25.21	9.142E+00	3.579E-01
17.25	1.687E+01	6.0	5.009E-01	25.95	7.661E+00	4.563E-01
17.71	2.088E+01	2.7	6.881E-01	26.64	9.498E+00	2.566E-01
18.25	2.158E+01	2.0	8.012E-01	27.44	9.839E+00	1.980E-01
18.67	1.918E+01	2.8	7.789E-01	28.07	8.760E+00	2.440E-01
19.20	1.766E+01	2.0	8.016E-01	28.86	8.085E+00	1.628E-01
19.75	1.608E+01	4.6	8.165E-01	29.68	7.381E+00	3.364E-01
20.25	1.105E+01	6.5	6.197E-01	30.42	5.086E+00	3.311E-01
20.75	9.029E+00	3.8	5.576E-01	31.16	4.165E+00	1.585E-01
21.73	6.798E+00	3.1	5.040E-01	32.62	3.152E+00	9.926E-02
22.25	6.100E+00	2.9	4.965E-01	33.38	2.836E+00	8.105E-02
23.25	4.679E+00	3.3	4.530E-01	34.86	2.187E+00	7.239E-02
23.72	4.447E+00	2.3	4.661E-01	35.56	2.084E+00	4.766E-02
24.14	3.973E+00	2.6	4.462E-01	36.18	1.867E+00	4.932E-02
24.65	3.595E+00	3.6	4.382E-01	36.93	1.694E+00	6.153E-02
25.17	2.889E+00	3.0	3.828E-01	37.70	1.366E+00	4.100E-02
25.74	2.896E+00	2.5	4.188E-01	38.53	1.374E+00	3.413E-02
26.25	2.496E+00	3.7	3.899E-01	39.28	1.188E+00	4.446E-02
26.75	2.165E+00	3.5	3.643E-01	40.02	1.034E+00	3.591E-02
27.25	1.849E+00	4.4	3.345E-01	40.75	8.853E-01	3.915E-02
27.75	1.547E+00	4.1	3.007E-01	41.48	7.435E-01	3.049E-02
28.23	1.289E+00	4.9	2.678E-01	42.18	6.212E-01	3.055E-02
28.75	9.743E-01	5.7	2.176E-01	42.94	4.713E-01	2.694E-02
29.25	8.663E-01	3.4	2.070E-01	43.67	4.206E-01	1.438E-02
29.74	7.485E-01	3.4	1.909E-01	44.38	3.646E-01	1.227E-02
30.15	6.839E-01	5.2	1.840E-01	44.98	3.342E-01	1.725E-02
30.64	5.546E-01	3.3	1.589E-01	45.69	2.719E-01	9.095E-03
31.21	5.348E-01	6.1	1.647E-01	46.52	2.634E-01	1.615E-02
32.25	3.741E-01	4.2	1.310E-01	48.03	1.857E-01	7.885E-03
32.75	3.166E-01	4.5	1.177E-01	48.75	1.578E-01	7.086E-03
33.75	2.530E-01	4.7	1.058E-01	50.19	1.271E-01	5.957E-03
34.25	1.930E-01	7.8	8.544E-02	50.91	9.735E-02	7.562E-03
35.25	1.167E-01	6.2	5.777E-02	52.35	5.934E-02	3.683E-03
35.75	9.994E-02	8.3	5.228E-02	53.06	5.106E-02	4.247E-03
36.14	5.889E-02	11.3	3.213E-02	53.62	3.019E-02	3.424E-03
36.64	4.875E-02	6.2	2.805E-02	54.33	2.510E-02	1.561E-03
37.14	6.256E-02	3.9	3.794E-02	55.05	3.235E-02	1.270E-03
37.75	5.908E-02	3.8	3.817E-02	55.91	3.073E-02	1.171E-03
38.25	5.422E-02	4.1	3.686E-02	56.62	2.833E-02	1.163E-03
38.75	4.623E-02	5.6	3.305E-02	57.33	2.427E-02	1.367E-03
39.25	3.252E-02	6.8	2.443E-02	58.04	1.715E-02	1.168E-03
39.75	3.200E-02	5.7	2.525E-02	58.75	1.696E-02	9.664E-04
40.25	2.228E-02	8.1	1.845E-02	59.45	1.187E-02	9.584E-04
40.75	1.760E-02	7.2	1.529E-02	60.15	9.421E-03	6.786E-04
41.25	1.812E-02	6.9	1.649E-02	60.86	9.744E-03	6.750E-04
41.75	1.179E-02	10.8	1.124E-02	61.56	6.372E-03	6.906E-04
42.14	8.532E-03	9.2	8.431E-03	62.10	4.631E-03	4.247E-04
42.64	9.560E-03	7.1	9.886E-03	62.80	5.216E-03	3.708E-04
43.75	7.580E-03	6.9	8.653E-03	64.35	4.184E-03	2.906E-04
44.25	7.965E-03	7.1	9.498E-03	65.04	4.420E-03	3.120E-04
45.25	6.582E-03	8.2	8.550E-03	66.43	3.693E-03	3.031E-04
45.75	5.624E-03	9.7	7.620E-03	67.12	3.173E-03	3.063E-04
46.75	3.353E-03	11.1	4.934E-03	68.49	1.913E-03	2.116E-04
47.25	3.693E-03	10.4	5.661E-03	69.18	2.119E-03	2.194E-04

SCATTERING OF 6-LI PARTICLES ON 40-CA

ELAB = 156.000 MEV   Q = 0.0 MEV   I = 0 +

ECM = 135.591 MEV   K = 5.8242/FERMI   ETA = 1.85545

LABORATORY DATA THETA DEGREE	SIGMA MB/SR	DSIGMA %	RUTHERFORD SIGMA/SR	CM DATA THETA DEGREE	SIGMA MB/SR	DSIGMA MB/SR
7.25	2.276E+03	1.1	1.910E-01	8.36	1.713E+03	1.835E+01
7.75	2.219E+03	8.6	2.430E-01	8.94	1.670E+03	1.431E+02
8.25	3.865E+02	48.8	5.433E-02	9.52	2.910E+02	1.422E+02
8.75	3.318E+02	6.9	5.900E-02	10.09	2.499E+02	1.737E+01
9.25	5.038E+02	4.6	1.118E-01	10.67	3.796E+02	1.741E+01
9.39	4.885E+02	3.5	1.151E-01	10.83	3.682E+02	1.295E+01
9.75	5.720E+02	3.2	1.566E-01	11.25	4.312E+02	1.388E+01
9.89	5.885E+02	3.8	1.706E-01	11.41	4.437E+02	1.705E+01
10.25	4.704E+02	4.3	1.572E-01	11.82	3.547E+02	1.527E+01
10.39	4.794E+02	4.5	1.692E-01	11.98	3.616E+02	1.616E+01
11.00	2.585E+02	14.2	1.145E-01	12.69	1.951E+02	2.763E+01
11.50	7.385E+01	31.6	3.906E-02	13.26	5.576E+01	1.761E+01
12.00	2.573E+01	24.7	1.613E-02	13.84	1.944E+01	4.799E+00
12.50	1.048E+01	46.6	7.731E-03	14.41	7.924E+00	3.691E+00
13.00	4.393E+01	12.2	3.788E-02	14.99	3.323E+01	4.061E+00
13.50	6.311E+01	3.7	6.324E-02	15.56	4.776E+01	1.749E+00
14.00	6.599E+01	3.0	7.642E-02	16.14	4.996E+01	1.519E+00
14.50	5.036E+01	6.7	6.706E-02	16.71	3.815E+01	2.552E+00
15.00	3.400E+01	9.5	5.182E-02	17.29	2.578E+01	2.458E+00
15.39	2.174E+01	14.4	3.670E-02	17.73	1.649E+01	2.371E+00
15.89	6.271E+00	32.5	1.202E-02	18.31	4.759E+00	1.549E+00
16.39	1.353E+00	49.2	2.932E-03	18.88	1.028E+00	5.054E-01
17.00	3.391E+00	14.7	8.497E-03	19.58	2.578E+00	3.798E-01
17.50	6.652E+00	8.7	1.870E-02	20.16	5.060E+00	4.412E-01
18.00	9.139E+00	5.1	2.873E-02	20.73	6.958E+00	3.565E-01
18.50	1.063E+01	4.3	3.725E-02	21.30	8.097E+00	3.482E-01
19.00	7.787E+00	7.8	3.034E-02	21.88	5.938E+00	4.652E-01
19.50	4.589E+00	13.5	1.982E-02	22.45	3.502E+00	4.727E-01
20.00	1.840E+00	20.7	8.786E-03	23.02	1.406E+00	2.908E-01
20.50	8.241E-01	13.4	4.338E-03	23.59	6.300E-01	8.418E-02
21.00	8.761E-01	10.5	5.073E-03	24.17	6.704E-01	7.012E-02
21.39	1.251E+00	8.1	7.792E-03	24.61	9.580E-01	7.736E-02
21.89	1.727E+00	3.7	1.178E-02	25.18	1.323E+00	4.953E-02
22.39	1.811E+00	3.7	1.351E-02	25.76	1.389E+00	5.094E-02
23.00	1.857E+00	3.4	1.540E-02	26.45	1.426E+00	4.877E-02
23.50	1.385E+00	7.8	1.250E-02	27.02	1.065E+00	8.319E-02
24.00	8.105E-01	10.8	7.952E-03	27.59	6.238E-01	6.740E-02
24.50	6.161E-01	7.7	6.556E-03	28.16	4.747E-01	3.657E-02
25.00	3.936E-01	7.7	4.535E-03	28.73	3.036E-01	2.326E-02
25.50	3.553E-01	8.0	4.426E-03	29.30	2.743E-01	2.187E-02
26.00	3.594E-01	4.7	4.832E-03	29.87	2.778E-01	1.319E-02
26.50	4.078E-01	4.3	5.909E-03	30.44	3.155E-01	1.363E-02
27.00	3.553E-01	7.8	5.540E-03	31.01	2.752E-01	2.159E-02
27.39	3.450E-01	5.8	5.692E-03	31.45	2.675E-01	1.553E-02
27.89	2.891E-01	6.7	5.120E-03	32.02	2.244E-01	1.497E-02
28.39	2.266E-01	9.3	4.303E-03	32.59	1.761E-01	1.643E-02
29.00	1.245E-01	12.6	2.569E-03	33.28	9.688E-02	1.217E-02
29.50	9.587E-02	10.4	2.115E-03	33.85	7.471E-02	7.798E-03
30.00	7.073E-02	13.1	1.667E-03	34.42	5.519E-02	7.254E-03
30.50	8.897E-02	11.2	2.236E-03	34.98	6.951E-02	7.763E-03
31.00	8.350E-02	10.0	2.236E-03	35.55	6.532E-02	6.506E-03
31.50	8.002E-02	11.5	2.281E-03	36.12	6.269E-02	7.234E-03
32.50	6.680E-02	10.5	2.151E-03	37.25	5.247E-02	5.515E-03
33.00	6.190E-02	12.9	2.115E-03	37.81	4.868E-02	6.271E-03
33.45	4.358E-02	23.5	1.570E-03	38.32	3.432E-02	8.069E-03
33.89	5.062E-02	16.5	1.918E-03	38.82	3.991E-02	6.595E-03
35.50	5.205E-02	15.6	2.362E-03	40.63	4.124E-02	6.441E-03
37.00	4.895E-02	17.0	2.606E-03	42.32	3.895E-02	6.624E-03
38.50	2.454E-02	22.8	1.523E-03	44.00	1.962E-02	4.479E-03
40.00	1.519E-02	12.4	1.092E-03	45.68	1.220E-02	1.518E-03
41.39	1.977E-02	9.9	1.620E-03	47.23	1.596E-02	1.584E-03
43.00	8.416E-03	14.8	7.979E-04	49.03	6.831E-03	1.009E-03
44.50	8.159E-03	15.1	8.813E-04	50.70	6.657E-03	1.004E-03

SCATTERING OF 6-LI PARTICLES ON 90-ZR

ELAB = 156.000 MEV   Q = 0.0 MEV   I = 0 +

ECM = 146.217 MEV   K = 6.2806/FERMI   ETA = 3.71089

LABORATORY DATA			RUTHERFORD	CM DATA		
THETA DEGREE	SIGMA MB/SR	DSIGMA %	SIGMA/SR	THETA DEGREE	SIGMA MB/SR	DSIGMA MB/SR
8.25	6.560E+03	8.5	2.298E-01	8.81	5.753E+03	4.918E+02
8.75	4.695E+03	9.6	2.080E-01	9.35	4.118E+03	3.955E+02
9.25	3.556E+03	9.1	1.967E-01	9.88	3.119E+03	2.833E+02
10.14	1.753E+03	14.6	1.399E-01	10.83	1.538E+03	2.248E+02
10.64	1.062E+03	14.9	1.027E-01	11.37	9.321E+02	1.387E+02
11.14	7.016E+02	11.2	8.148E-02	11.90	6.159E+02	6.868E+01
11.64	5.423E+02	6.5	7.503E-02	12.43	4.762E+02	3.111E+01
12.14	4.691E+02	6.2	7.675E-02	12.97	4.120E+02	2.566E+01
13.25	2.033E+02	14.7	4.714E-02	14.15	1.787E+02	2.620E+01
13.75	1.280E+02	14.9	3.438E-02	14.68	1.125E+02	1.674E+01
14.25	7.876E+01	11.9	2.439E-02	15.22	6.925E+01	8.234E+00
14.75	6.674E+01	4.6	2.371E-02	15.75	5.870E+01	2.697E+00
15.25	7.148E+01	3.6	2.899E-02	16.28	6.288E+01	2.237E+00
15.75	6.155E+01	3.4	2.838E-02	16.82	5.417E+01	1.825E+00
16.25	5.917E+01	8.5	3.089E-02	17.35	5.209E+01	4.432E+00
16.75	2.830E+01	26.4	1.666E-02	17.88	2.492E+01	6.585E+00
17.14	1.356E+01	28.2	8.753E-03	18.30	1.195E+01	3.370E+00
17.64	7.111E+00	15.4	5.143E-03	18.83	6.266E+00	9.648E-01
18.14	6.717E+00	10.4	5.428E-03	19.36	5.920E+00	6.148E-01
18.75	1.128E+01	8.6	1.039E-02	20.01	9.949E+00	8.568E-01
19.25	9.016E+00	9.4	9.220E-03	20.55	7.954E+00	7.464E-01
19.75	6.220E+00	17.8	7.041E-03	21.08	5.489E+00	9.770E-01
20.25	3.350E+00	23.2	4.187E-03	21.61	2.958E+00	6.875E-01
20.75	1.224E+00	38.1	1.685E-03	22.14	1.081E+00	4.117E-01
21.25	4.238E-01	61.2	6.409E-04	22.68	3.745E-01	2.292E-01
21.75	1.259E+00	14.5	2.087E-03	23.21	1.113E+00	1.615E-01
22.25	1.345E+00	14.5	2.439E-03	23.74	1.190E+00	1.728E-01
22.75	2.465E+00	13.9	4.881E-03	24.27	2.181E+00	3.039E-01
23.14	1.819E+00	22.3	3.851E-03	24.69	1.610E+00	3.586E-01
23.64	5.070E-01	53.4	1.168E-03	25.22	4.489E-01	2.397E-01
24.14	1.228E-01	60.6	3.072E-04	25.75	1.088E-01	6.591E-02
24.75	1.703E-01	41.7	4.701E-04	26.40	1.510E-01	6.300E-02
25.25	1.110E-01	43.8	3.314E-04	26.93	9.842E-02	4.310E-02
25.75	2.428E-01	26.1	7.831E-04	27.46	2.154E-01	5.619E-02
26.25	3.647E-01	30.8	1.269E-03	27.99	3.238E-01	9.959E-02
26.75	3.384E-01	23.1	1.268E-03	28.52	3.006E-01	6.955E-02
27.25	1.988E-01	32.7	8.009E-04	29.05	1.766E-01	5.769E-02
27.75	5.693E-02	82.0	2.463E-04	29.58	5.062E-02	4.150E-02
28.25	4.136E-02	58.1	1.920E-04	30.11	3.680E-02	2.136E-02
28.75	4.264E-02	63.4	2.120E-04	30.64	3.796E-02	2.405E-02
29.14	3.566E-02	31.1	1.869E-04	31.06	3.176E-02	9.862E-03
30.75	9.450E-02	18.1	6.111E-04	32.76	8.432E-02	1.527E-02
32.25	5.966E-03	112.3	4.645E-05	34.35	5.333E-03	5.990E-03
33.75	2.156E-02	36.4	2.003E-04	35.94	1.931E-02	7.021E-03

SCATTERING OF 6-LI PARTICLES ON 208-PB

ELAB = 156.000 MEV   Q = 0.0 MEV   I = 0 +

ECM = 151.615 MEV   K = 6.5125/FERMI   ETA = 7.60734

LABORATORY DATA			RUTHERFORD	CM DATA		
THETA DEGREE	SIGMA MB/SR	DSIGMA %	SIGMA/SR	THETA DEGREE	SIGMA MB/SR	DSIGMA MB/SR
9.64	5.402E+04	6.0	8.369E-01	9.93	5.099E+04	3.081E+03
10.14	3.783E+04	7.2	7.172E-01	10.44	3.571E+04	2.581E+03
10.64	2.670E+04	6.5	6.133E-01	10.95	2.521E+04	1.649E+03
11.25	1.898E+04	4.9	5.445E-01	11.58	1.792E+04	8.808E+02
11.75	1.600E+04	4.7	5.459E-01	12.10	1.511E+04	7.038E+02
12.25	1.156E+04	7.5	4.655E-01	12.61	1.091E+04	8.225E+02
12.75	7.452E+03	9.3	3.521E-01	13.13	7.039E+03	6.547E+02
13.25	4.632E+03	7.8	2.551E-01	13.64	4.375E+03	3.432E+02
13.75	3.833E+03	3.6	2.446E-01	14.15	3.621E+03	1.317E+02
14.25	3.259E+03	5.2	2.398E-01	14.67	3.079E+03	1.595E+02
14.75	2.156E+03	8.0	1.820E-01	15.18	2.038E+03	1.636E+02
15.25	1.540E+03	7.8	1.483E-01	15.70	1.455E+03	1.129E+02
15.64	1.097E+03	8.1	1.168E-01	16.10	1.036E+03	8.402E+01
16.14	7.804E+02	5.9	9.421E-02	16.61	7.377E+02	4.381E+01
16.64	6.370E+02	3.2	8.680E-02	17.13	6.022E+02	1.899E+01
17.25	5.747E+02	5.5	9.035E-02	17.75	5.435E+02	2.980E+01
17.75	4.236E+02	6.6	7.460E-02	18.27	4.007E+02	2.646E+01
18.25	2.987E+02	4.5	5.872E-02	18.78	2.825E+02	1.258E+01
18.75	1.928E+02	6.8	4.220E-02	19.30	1.824E+02	1.232E+01
19.25	1.267E+02	7.2	3.078E-02	19.81	1.199E+02	8.577E+00
19.75	1.066E+02	7.7	2.867E-02	20.33	1.009E+02	7.782E+00
20.25	9.354E+01	4.9	2.777E-02	20.84	8.854E+01	4.368E+00
20.75	7.004E+01	6.4	2.290E-02	21.35	6.631E+01	4.229E+00
21.25	5.196E+01	7.3	1.867E-02	21.87	4.920E+01	3.590E+00
21.64	3.571E+01	8.9	1.378E-02	22.27	3.382E+01	2.999E+00
22.14	2.800E+01	5.5	1.183E-02	22.78	2.652E+01	1.457E+00
22.64	2.229E+01	5.5	1.029E-02	23.30	2.112E+01	1.153E+00
23.25	1.826E+01	7.8	9.358E-03	23.92	1.730E+01	1.349E+00
23.75	1.345E+01	7.5	7.495E-03	24.44	1.275E+01	9.534E-01
24.25	1.038E+01	8.8	6.282E-03	24.95	9.844E+00	8.646E-01
24.75	7.255E+00	10.7	4.757E-03	25.46	6.880E+00	7.375E-01
25.25	5.579E+00	7.4	3.958E-03	25.98	5.291E+00	3.939E-01
25.75	4.780E+00	9.1	3.663E-03	26.49	4.535E+00	4.130E-01
26.25	4.086E+00	12.0	3.376E-03	27.00	3.877E+00	4.657E-01
26.75	2.539E+00	13.5	2.260E-03	27.52	2.410E+00	3.242E-01
27.25	1.782E+00	15.8	1.706E-03	28.03	1.692E+00	2.672E-01
27.64	1.190E+00	20.2	1.204E-03	28.43	1.129E+00	2.282E-01
28.14	1.212E+00	10.6	1.315E-03	28.94	1.151E+00	1.214E-01
29.25	2.377E-01	85.9	3.003E-04	30.08	2.258E-01	1.939E-01
29.75	5.116E-01	20.4	6.906E-04	30.59	4.863E-01	9.904E-02
30.75	1.569E-01	55.9	2.409E-04	31.62	1.492E-01	8.333E-02
32.25	2.963E-01	34.9	5.481E-04	33.16	2.820E-01	9.829E-02